
Membrane Transport, Structure, Function, and Biogenesis:

# New Roles of Myosin II during Vesicle Transport and Fusion in Chromaffin Cells

Patricia Ñeco, Daniel Giner, Salvador Viniegra, Ricardo Borges, Alvaro Villarroel and Luis M. Gutiérrez

*J. Biol. Chem. 2004, 279:27450-27457.*
*doi: 10.1074/jbc.M311462200 originally published online April 6, 2004*

THE JOURNAL OF BIOLOGICAL CHEMISTRY
Vol. 279, No. 26, Issue of June 25, pp. 27450–27457, 2004

*Printed in U.S.A.*

# New Roles of Myosin II during Vesicle Transport and Fusion in Chromaffin Cells*

Received for publication, October 20, 2003, and in revised form, March 16, 2004
Published, JBC Papers in Press, April 6, 2004, DOI 10.1074/jbc.M311462200

**Patricia Ñeco‡§, Daniel Giner‡¶, Salvador Viniegra‡, Ricardo Borges‖, Alvaro Villarroel**, and Luis M. Gutiérrez‡ ‡‡**

*From the ‡Instituto de Neurociencias, Centro Mixto CSIC-Universidad Miguel Hernández, E-03550 Alicante, Spain, the ‖Unidad de Farmacología, Facultad de Medicina Universidad de la Laguna, E-38071 Tenerife, Spain, and the **Instituto Cajal, CSIC, E28002 Madrid, Spain*

**Modified herpes virus (amplicons) were used to express myosin regulatory light chain (RLC) chimeras with green fluorescent protein (GFP) in cultured bovine chromaffin cells to study myosin II implication in secretion. After infection, RLC-GFP constructs were clearly identified in the cytoplasm and accumulated in the cortical region, forming a complex network that co-localized with cortical F-actin. Cells expressing wild type RLC-GFP maintained normal vesicle mobility, whereas cells expressing an unphosphorylatable form (T18A/S19A RLC-GFP) presented severe restrictions in granule movement as measured by individual tracking in dynamic confocal microscopy studies. Interestingly, the overexpression of this mutant form of RLC also affected the initial secretory burst elicited by either high $K^+$ or $BaCl_2$, as well as the secretion induced by fast release of calcium from caged compounds in individual cells. Moreover, T18A/S19A RLC-GFP-infected cells presented slower fusion kinetics of individual granules compared with controls as measured by analysis of amperometric spikes. Taken together, our results demonstrate the implication of myosin II in the transport of vesicles, and, surprisingly, in the final phases of exocytosis involving transitions affecting the activity of docked granules, and therefore uncovering a new role for this cytoskeletal element.**

Neuroendocrine chromaffin cells have been widely used as a model to study exocytosis of dense vesicles. These cells release catecholamines in a calcium-dependent process involving granule transport, translocation, docking to the active sites and finally, membrane fusion with extrusion of soluble contents by exocytosis (1). Cytoskeletal proteins play an essential role among the cytosolic elements organizing the transport of vesicles from the internal regions where chromaffin granule biogenesis takes place toward the subcortical region where they are stored to form a reserve pool to sustain continuous stimulation (2). In this sense, peripheral F-actin forming a network layer beneath the plasma membrane constitutes a barrier that excludes vesicle access to release sites (3). Upon stimulation and calcium influx, a local and transient disruption of this network occurs (4), allowing vesicle access to the immediate subplasmalemmal area. Therefore, molecular motors associated with F-actin trails would be necessary to conduct vesicles throughout regions with different F-actin organization. A number of observations suggest that conventional myosin II activity influences catecholamine secretion. For example, chromaffin cell stimulation induces the calcium-dependent phosphorylation of the regulatory subunit of myosin light chain (RLC)[1] (5–7), and as such, constitutes the basic mechanism for governing the interaction of non-muscular myosin II with actin (8). In addition, phosphorylation of non-muscle myosins by the specific enzyme myosin light chain kinase (MLCK), may be essential to this proteins role in secretion, because inhibition of MLCK by a variety of chemicals abrogates secretion in permeabilized (9–12) or intact chromaffin cells (2). Nevertheless, the relatively low specificity of most of the myosin inhibitors employed, and furthermore, the demonstration that other myosin forms, such as unconventional myosin V, may also participate in vesicle transport and secretion in chromaffin (13) or PC 12 cells (14), makes use of alternative experimental strategies desirable in study of a specific role for myosin II in secretion. The expression of RLC and its unphosphorylatable double mutant were used to demonstrate the participation of myosin II in mitosis and cytokinesis (15). We have used this strategy in combination with dynamic confocal microscopy and single cell amperometry to demonstrate myosin II participation in different steps of the secretory cascade. Our data suggest that, in addition to the traditional role of myosin II in vesicle transport, this motor protein influences the very final events of membrane fusion, therefore unmasking a previously unknown role.

## EXPERIMENTAL PROCEDURES

*Materials*—Oligonucleotides were synthesized by Genotech. *Taq* DNA polymerase was obtained from BioTools, Madrid. Ligase and restriction endonucleases were purchased from Fermentas, St. Leon-Rot, Germany. All of other reagents were purchased from Sigma.

*Production of Wild Type and Mutant Forms of RLC-GFP Constructs*—A plasmid encoding chicken gizzard smooth muscle RLC (a gift of Dr. Kendrick-Jones, MRC, Cambridge, UK) was used for site-directed PCR cassette mutagenesis. The modifications were confirmed by sequencing in both directions.

pRLC-wt-GFP and pRLC-T18A/S19A-GFP were generated using pEGFP-N1 (Clontech). The final construct was obtained by NheI/MunI digestion and inserted into a XbaI/EcoRI-digested pHSVpuc amplicon,

* This work was supported in part by Spanish Ministry of Science and Technology Grant BMC2002-00845 and Generalitat Valenciana Grant GRUPOS03/040. The costs of publication of this article were defrayed in part by the payment of page charges. This article must therefore be hereby marked "*advertisement*" in accordance with 18 U.S.C. Section 1734 solely to indicate this fact.

§ Recipient of a fellowship from the Generalitat Valenciana.

¶ Recipient of a fellowship from the Spanish Ministry of Science and Technology.

‡‡ To whom correspondence should be addressed: Instituto de Neurociencias, Centro Mixto CSIC-Universidad Miguel Hernández, Campus de San Juan, 03550 Alicante, Spain. Tel.: 34-96-5919563; Fax: 34-96-5919484; E-mail: luisguti@umh.es.

[1] The abbreviations used are: RLC, regulatory light chain; MLCK, myosin light chain kinase; GFP, green fluorescent protein; HSV, herpes simplex virus; MSD, mean square distance; PBS, phosphate-buffered saline.

upstream of the IE 4/5 promoter. Packaging and amplification of this vector were performed using standard procedures (16).

*Chromaffin Cell Preparation and Infection*—Chromaffin cells were prepared from bovine adrenal glands by collagenase digestion and further separated from debris and erythrocytes by centrifugation on Percoll gradients as described (12, 17). Cells were suspended in Dulbecco's modified Eagle's medium supplemented with 10% fetal calf serum, 10 $\mu$M cytosine arabinoside, 10 $\mu$M fluorodeoxyuridine, 50 IU/ml penicillin, and 50 $\mu$g/ml streptomycin. For flash photolysis and amperometrical experiments, cells were plated on 28- and 12-mm diameter glass coverslips, respectively, at a density of $5 \times 10^5$ cells/well and for confocal microscopy studies, cells were plated in 35-mm diameter Petri dishes (Corning Inc., Corning, NY) at the same density.

Primary cultures of chromaffin cells were infected with a herpes simplex virus (HSV-1) amplicon containing the constructs described above. Efficiency of virus infection was determined by fluorescent microscopy, using serial dilutions of purified virus. The dilution chosen for further experiments (20–30 $\mu$l virus per 1 ml of medium) produced 10–15% infection efficiency. GFP fluorescence was observed 1 day after infection and persisted, at least, along the two following days. Amperometric measurements were carried out during this time.

*Amperometric Detection of Secretion in Individual Chromaffin Cells*—Secretory activity in non-infected and infected single chromaffin cells was studied at room temperature (21–22 °C) and stimulating the cells by superfusion with depolarizing 59 mM potassium as described (18–20). Briefly, we prepared microelectrodes by insulating 11-$\mu$m diameter carbon fibers with polypropylene. Electrochemical recordings were performed using an Axopatch 200A and 200B (Axon Instruments, Foster City, CA). Oxidized current was filtered at a corner frequency of 400 Hz using a 8-poles low-pass Bessel filter and acquired at 5 KHz. Electrodes were backfilled with mercury to connect to the headstage. Carbon electrodes are gently placed onto the cell membrane using high precision hydraulic micromanipulation and assessing cell membrane deformation with an Axiovert 135 inverted-stage microscope (Zeiss, Oberkochen, Germany) mounting Hoffman optics (Modulation Optics, Greenvale, NY). Cells were bathed in a Krebs-HEPES solution containing (in mmol/liter): NaCl (140), KCl (5), $MgCl_2$ (1.2), $CaCl_2$ (2), HEPES (10), glucose (11), and the pH adjusted to 7.4 using a NaOH solution. Cells were stimulated by superfusion with depolarizing (59 mM high potassium solution obtained by replacing isosmotically NaCl by KCl) or 5 mM $BaCl_2$ solutions and applied through a valve-controlled puffer tip commanded by the acquisition software and disposed near the studied cells.

Microelectrodes employed in experiments to study individual events were prepared with 11-$\mu$m diameter carbon fiber in glass as previously described (21), and polished at a 45° angle on a diamond dust-embedded micropipette beveling wheel. These electrodes were calibrated using a flow-injection system with 50 $\mu$M norepinephrine. Secretion is elicited by a 5-s pulse of a secretagogue (5 mM BaCl) from a glass micropipette located 40 $\mu$m from the cell. Individual spike analysis was performed using macros for IGOR (Wavemetrics, Lake Oswego, OR), allowing for peak detection, integration, and kinetic parameter calculations (22). Electrode variations were alleviated by using the same electrode for measurements in control (non-infected) and infected cells.

*Flash-photolysis Experiments*—Photorelease of calcium from caged compounds was done using a 5 $\mu$M concentration of *o*-nitrophenyl-EGTA-AM (Molecular Probes, Eugene, OR) in Krebs-HEPES buffer and incubated 30 min, after 3 washes, the glass coverslip containing the cells was mounted in the stage of a Zeiss Axiovert 100S inverted microscope using a ×100 Plan-Neofluar objective. In this system a dual-port condenser allowed excitation of the specimen with a monochromator Polychrome IV (8% incoming light, Till-Photonics, Munich, Germany) and simultaneous application of a 5-ms UV flash using a pulsed Xenon arc lamp system (92% incoming light, UV Flash II, Till-Photonics), therefore allowing $[Ca^{2+}]_i$ measurements using Fura 2 excitation at 340/380 nm (for this purpose 4 $\mu$M Fura 2-AM was incubated simultaneously with the *o*-nitrophenyl-EGTA). Fluorescence emission from a 20 × 20-$\mu$m restricted area (Viewfinder III, Till-Photonics) was detected in a photomultiplier tube (Hamamatsu Inc., Hamamatsu, Japan). Control of excitation light and acquisition were performed through PClamp 8.0 software (Axon Instruments) in a PC computer. Calculation of $[Ca^{2+}]_i$ was performed using a dissociation constant of 224 nM for Fura 2 (23), with minor corrections after application of the flash (24). In all the experiments, a second flash was given to assess that no further calcium was released and the trace obtained was subtracted from the first flash to eliminate the flash artifact (see significance of this procedure in Fig. 6). Calcium elevation causes a rapid release of vesicles in control or wild type RLC-GFP expressing cells as detected by amperometry (Fig. 6*A*, example trace).

*Dynamic Confocal Microscopy Studies of Chromaffin Granule Mobility and RLC-GFP Expression*—Infected cells expressing the RLC-GFP constructs were labeled with 4 $\mu$M quinacrine for 10 min and vesicle movements were studied by dynamic confocal microscopy as described elsewhere (2, 12). Briefly, fluorescent emission from quinacrine trapped in the acidic vesicles was investigated using an Olympus Fluoview FV300 confocal laser system and a BX-50 WI up-right microscope incorporating a ×100 LUMPlan FI water-immersion objective. This system allows for *z* axis reconstruction (0.5-$\mu$m *z* slice) and time lapse dynamic studies with time resolutions ranging from 0.1 s for 200 × 150 pixel image acquisition (adequate for region studies) to about 0.6 s for images of 400 × 300 pixels (for visualization of the entire cell). Analysis of frames was performed using the public domain program ImageJ with Plugins for *x*/*y* displacement calculations of particle centroid, region of interest measurement, and image average and comparison. Mean square displacement (MSD) and diffusion coefficient calculations were performed using the equations described by Qian *et al.* (25).

In some experiments, labeling of F-actin in permeabilized and delipided cells was performed as described (20, 26). Briefly, after fixation, cells were incubated with 1 $\mu$M phalloidin-rhodamine (Molecular Probes, Eugene, OR) during 30 min in phosphate-buffered saline. After extensive washes, the samples were visualized in the confocal microscope.

The Student's *t* test for unpaired samples, the Mann-Whitney non-parametric test, or the two-way analysis of variance tests were used to establish statistical significance among the different experimental data (samples were considered significantly different when $p < 0.05$). All data were expressed as mean ± S.E. from experiments performed in a number ($n$) of individual cells or wells. Presented data represents experiments performed with cells from at least three different cultures.

## RESULTS

*Expression of Myosin Regulatory Light Chain Constructs with GFP in Bovine Chromaffin Cells*—To study the role of myosin II during chromaffin cell secretion, we expressed wild type and unphosphorylatable myosin RLC (15). An amplicon viral infection system was employed to express RLC linked by its N terminus to enhanced RLC-GFP in chromaffin cells following a strategy that has been successful for other proteins (19, 27). Under these conditions, infection of cultured bovine chromaffin cells resulted in the expression of the RLC-GFP constructs in 10–15% of the cells. Confocal microscopy of cells overexpressing wild type or the unphosphorylatable T18A/S19A RLC-GFP revealed a similar cellular distribution in the nucleus, cytoplasm, and cell periphery (Fig. 1*A*). Interestingly, RLC-GFP constructs in the cytoplasm formed a network that extended from perinuclear to subplasmalemmal regions, where the protein was also concentrated (Fig. 1*B*). F-actin staining with phalloidin-rhodamine demonstrated a clear co-localization of peripheral RLC-GFP (Fig. 1*C*) and cortical F-actin (Fig. 1*D*), as observed by the intense yellow color indicating superposition of both channels detected sequentially during confocal imaging of a cell expressing the T18A/S19A construct (Fig. 1*E*). This data suggests that exogenous RLC might be associated with the endogenous myosin II heavy chain, because myosin II immunostaining has been shown to be linked to cortical F-actin, whereas myosin V appears to be preferentially distributed in the cell interior (12, 13).

*Expression of Unphosphorylatable Forms of RLC Affects Vesicle Transport in the Cytoplasm of Chromaffin Cells*—Would the expression of RLC-GFP constructs affect granule transport properties in the cytoplasm of chromaffin cells? To answer this question the dynamics of quinacrine-loaded dense granules was studied using confocal microscopy (2, 12). The high intensity fluorescence of moving granules can be easily visualized and tracked in the cytoplasm of cells expressing wild type RLC-GFP (Fig. 2*A*). The elevated mobility of granules in these time-lapse images taken one per second during 1 min is clearly indicated by the calculation of the average frame that produced

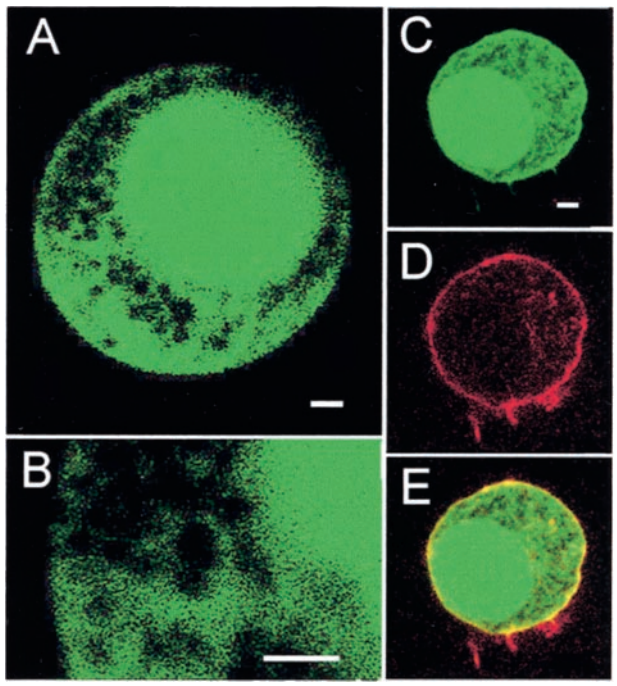


FIG. 1. **Cellular distribution of RLC-GFP constructs in chromaffin cells infected with amplicons.** Cells overexpressing wild type RLC-GFP and the double mutant T18A/S19A RLC-GFP were studied by laser confocal microscopy. Depicted are cells expressing the wild type chimera (*panel A*), and an enhanced detail of a cytoplasmic zone (*panel B*). *Panel C* shows a cell expressing T18A/S19A RLC-GFP. This cell was labeled with phalloidin-rhodamine (*panel D*), and *panel E* depicts the overlapped images of both channels acquired sequentially. These images are representative of experiments performed with dozens of cells from two different cultures. *Bars* represent 1 $\mu$m.

blurry images of the granule trajectories adopted during the observation time as depicted in Fig. 2*B*. Another method to assess the mobility of these vesicles is to draw a region of interest box and measure fluorescence variations because of the presence of granules, as indicated by the *arrow* in Fig. 2*A*. The fluctuations in fluorescence reflect the tendency of vesicles to enter and leave the confocal plane in periods lasting from 3 to 7 s, in a way that was similar to the mobility of vesicles in control uninfected cells (2). Conversely, relatively static granules were observed in the time-lapse images of cells expressing the unphosphorylatable T18A/S19A RLC-GFP construct (Fig. 2*C*). This figure shows granules that did not move between frames (10-s intervals are depicted). The average frame depicted unchanged granule positions that localized over the network of static RLC-GFP fluorescence as can be clearly seen in Fig. 2*D*. Region of interest analysis showed minor fluorescence fluctuations compared with mobile granules (Fig. 2*E*).

Further quantification of this reduction in vesicle mobility was obtained by tracking vesicles and studying their *xy* positions. Fig. 3*A* depicts an example of vesicle displacement in wild type RLC-GFP expressing cells. Using this type of data corresponding to 48 vesicles staying in the confocal plane for more than 10 s and from 9 different cells, we obtained the MSD at different time intervals and these values were averaged to generate the MSD *versus* time plot. Assuming that movement is governed by a single coefficient of diffusion, its value can be derived from the fitted slope (slope = $4 \times D$) (25). The diffusion coefficient was calculated to be $10.1 \pm 1 \times 10^{-3}$ $\mu m^2/s$ for RLC-GFP moving granules, similar to the coefficient calculated for granules in uninfected control cells ($8.68 \pm 0.99 \times 10^{-3}$ $\mu m^2/s$, $n = 27$ vesicles from 10 cells). As shown previously, overexpression of the T18A/S19A RLC-GFP construct results in a drastic change in vesicle mobility. An example of this restricted granule movement is shown in Fig. 3*B*. MSD calculations and representation for the different intervals showed a severe reduction in the slope and theoretical coefficient of diffusion that was estimated to be $0.32 \pm 0.02 \times 10^{-3}$ $\mu m^2/s$ ($n = 44$ vesicles from 10 cells), 20 times lower that in cells expressing the wild type form of myosin RLC. This reduction in vesicle mobility was similar to that caused by incubation of the control cells with 1 $\mu$M of the F-actin stabilizing agent phalloidin during 30 min (Fig. 3*B*). Phalloidin treatment reduced the apparent coefficient of diffusion to $0.24 \pm 0.01 \times 10^{-3}$ $\mu m^2/s$ ($n = 29$ vesicles from 6 cells). We also tested the effect of control cell incubation with the protein kinase C inhibitor staurosporine (1 $\mu$M, 30 min), which resulted in normal vesicle transport activity with a diffusion coefficient of $8.4 \pm 0.2 \times 10^{-3}$ $\mu m^2/s$ ($n = 24$ vesicles, from 10 cells, Fig. 3*B*), indicating that protein kinase C-dependent phosphorylation of RLC residues such as serines 1 or 2 does not seem to be implicated in the regulation of vesicle transport by this protein in neuroendocrine cells (28).

*Secretion Induced by Different Secretagogues Decreased in Cells Expressing Unphosphorylatable GFP-RLC*—What would be the impact on secretion produced by this drastic reduction in vesicle motion? Chromaffin cells expressing these constructs were tested for their ability to secrete catecholamines in response to different stimuli. Continuous cell depolarization by superfusion with a 59 mM KCl solution resulted in the release of individual vesicles as assessed by single cell amperometry. Secretion in control non-fluorescent cells was characterized by an initial burst of secretion lasting for 20 s followed by a sustained phase of slower secretion after that period (Fig. 4*A*). Using cumulative histograms of amperometric events corresponding to individual responses, we could obtain the average profile of secretion for 25 cells corresponding to 4 different cultures, as shown in Fig. 4*B* ($29 \pm 4$ vesicles fused 60 s after initiating depolarization). Expression of the wild type RLC-GFP construct resulted in very similar profiles of depolarizing evoked responses, that on average were not reduced in a statistically significant manner when compared with control cells (Fig. 4*B*, $28 \pm 5$ vesicles fused during 60 s, $n = 30$ cells). Instead, chromaffin cells expressing the T18A/S19A RLC-GFP construct showed a clear reduction in their capability to secrete catecholamines by direct depolarization as shown in the example of Fig. 4*A*. The averaged profile of secretion corresponding to 40 individual responses indicated a 40% reduction in the total number of vesicles fused during the first minute ($17 \pm 2$ vesicles) of continuous depolarization. Interestingly, this reduction in the number of fused vesicles affected both the initial burst and the late phase of release. Hence, the initial rate of release changed from $0.68 \pm 0.02$ vesicles fused/s in cells expressing wild type RLC-GFP to $0.27 \pm 0.02$ vesicles fused/s in T18A/S19A RLC-GFP expressing cells ($p < 0.0001$ using Student's $t$ test, the slope was calculated using data gathered during the initial 10 s). This result was somewhat surprising because myosin II was expected to alter the transport of vesicles, thereby affecting only the slow phases of secretion, leaving the release of fast secretory components of docked vesicles unaffected.

Furthermore, the use of an alternative secretagogue, such as $BaCl_2$, produced similar results, as the expression of the T18A/S19A RLC-GFP construct reduced secretion to half of the response obtained in cells expressing the wild type RLC-GFP construct as shown in Fig. 5 ($21 \pm 3$ vesicles fused at 1 min, $n = 33$ cells). The profile of secretion obtained with this secretory agent was affected by the expression of the unphosphorylatable form of myosin II RLC, and both initial and slow phases of secretion presented a statistically significant reduction in the number of vesicle fusions forming part of these kinetically

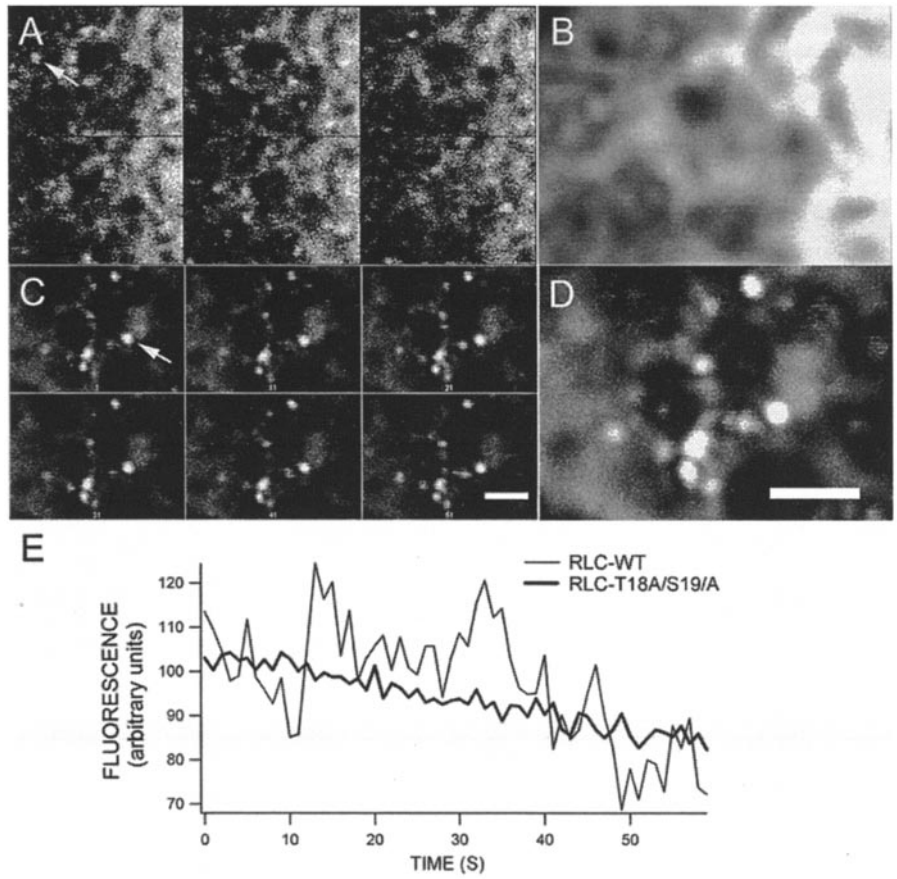


FIG. 2. **Vesicle mobility observed by dynamic confocal microscopy in chromaffin cells expressing RLC-GFP constructs.** Chromaffin cells were incubated with 4 $\mu$M quinacrine for 10 min and granules were visualized by dynamic confocal microscopy as indicated under "Experimental Procedures." *A*, time series of confocal images taken at 10-s intervals from a cell expressing wild type (*WT*) RLC-GFP. *B*, averaged image from 60 frames taken at 1 Hz of the same cell depicted in *panel A*. The blurry image demonstrates vesicle movements during image acquisition. *C*, frames obtained as in *panel A* from a cell expressing T18A/S19A RLC-GFP. *D*, averaged image of the cell expressing the T18A/S19A RLC-GFP construct. The crispy image is an indication of the restriction of movement of vesicles in this experiment. *E*, fluorescence changes of a region of interest measuring the presence of the vesicles indicated by *arrows* in the cells expressing the wild type (indicated in *panel A*) and unphosphorylatable form T18A/S19A RLC-GFP (indicated in *panel C*). *Scale bars* represent 1 $\mu$m.

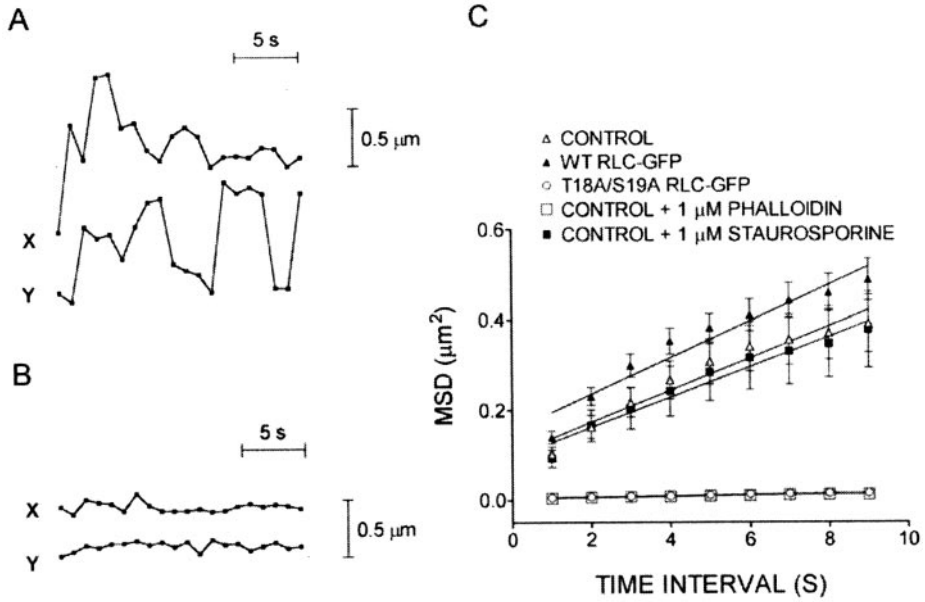


FIG. 3. **Tracking granule movements and calculation of diffusion coefficients in cells expressing RLC-GFP constructs.** Vesicles movements in the *xy* plane were tracked using specialized software determining particle centroid. *A*, depicted are typical examples of determined *xy* positions *versus* time for vesicles moving in wild type (*WT*) RLC-GFP expressing cells and also in cells expressing the T18A/S19A RLC-GFP construct. *B*, average of the MSD moved during the time intervals expressed in the *abscissa*, for 27 vesicles in 10 control uninfected cells, 48 vesicles corresponding to 9 wild type RLC-GFP expressing cells, and 44 granules from 10 cells expressing T18A/S19A RLC-GFP. In addition, the given MSD *versus* time plots for control cells treated with 1 $\mu$M phalloidin (29 granules from 6 cells) or 1 $\mu$M staurosporine during 30 min (24 vesicles from 10 cells) are shown. Also plotted were the best linear fits for the different curves, used to estimate the diffusion coefficient according to Qian *et al.* (25).

distinct secretory components (9 ± 1 vesicles released at 1 min, $n$ = 22 cells). There was a highly significant ($p < 0.0001$) reduction in the rate of release, estimated during the initial 10 s, from 0.61 ± 0.02 (wild type RLC-GFP) to 0.19 ± 0.01 vesicles fused/s (T18A/S19A RLC-GFP).

*Unphosphorylatable RLC Overexpression Affects the Fast Release Produced by Uncaged Calcium*—To further assess the alteration of the initial phases of secretion in cells expressing the mutated form of RLC-GFP, we conceived experiments using fast release of caged calcium. Cells were incubated with a 5 $\mu$M concentration of *o*-nitrophenyl-EGTA-AM (29) during 30 min. After an intense 5-ms flash, uncaged calcium produced a rapid elevation of $[Ca^{2+}]_i$ from basal levels of 80–140 nM as assessed using Fura 2-AM, to an estimated 900 ± 400 nM ($n$ = 24 cells). This elevation caused a rapid release of vesicles in control and wild type RLC-GFP expressing cells as detected by amperometry (Fig. 6*A*, example trace). A second flash (post-flash) was given to assess total release of caged calcium in the first trial, and no further secretion was detected as shown in the example of Fig. 6. This post-flash recording was subtracted from the first recording leaving the net amperometric response (Fig. 6*A*). The averaged cumulative response was obtained

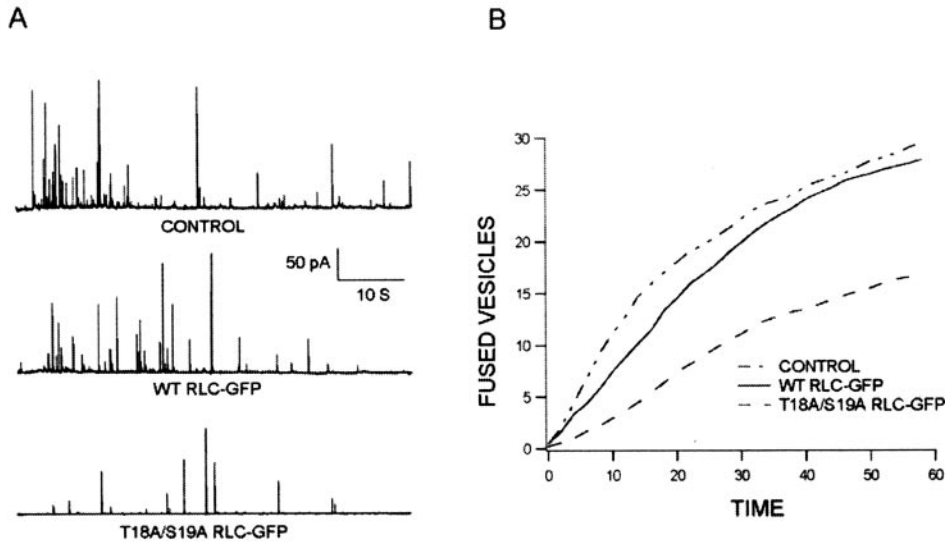


FIG. 4. **Secretory activity of chromaffin cells infected with amplicons containing myosin II RLC-GFP constructs.** Secretion was monitored by amperometry using 10-$\mu$m carbon-fiber electrodes in close apposition to the cell surface. *A*, amperometric traces representative from experiments performed in uninfected and amplicon-infected cells. Traces obtained from uninfected cells (*upper trace*), cells expressing wild type RLC-GFP (*middle trace*), and cells expressing T18A/S19A RLC-GFP (*lower trace*). Stimulation was performed by rapid superfusion during 1 min with a 59 mM KCl solution. *B*, cumulative event analysis. Conditions were as described in *panel A*, after building of event cumulative curves for individual cells. The average secretion was obtained from control uninfected ($n$ = 25 cells), wild type (*WT*) RLC-GFP ($n$ = 30 cells), and cells expressing T18A/S19A RLC-GFP GFP ($n$ = 40 cells).

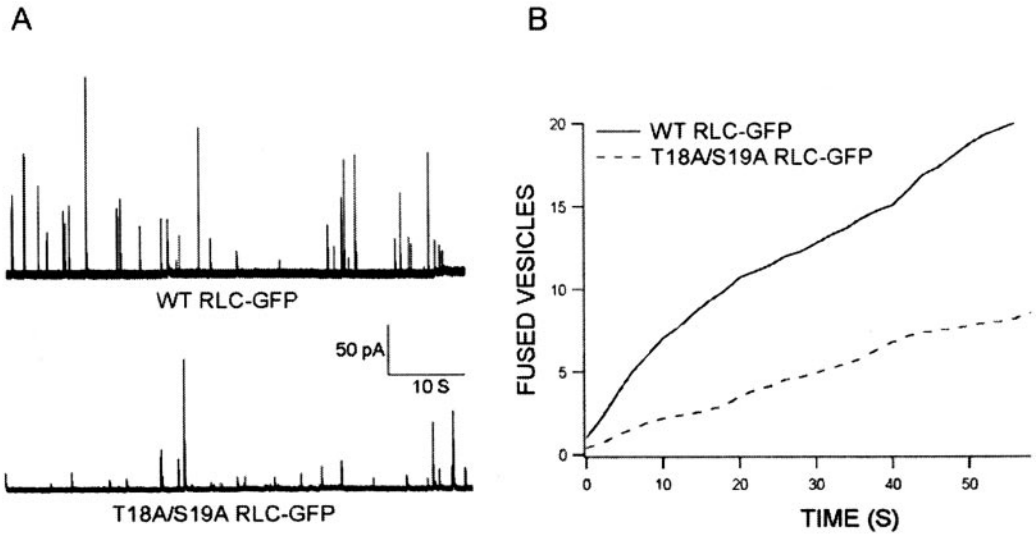


FIG. 5. **Barium-induced secretion from cells expressing RLC-GFP constructs.** Secretion was elicited by superfusion with 5 mM $BaCl_2$ in K/H basal buffer and studied by single cell amperometry as indicated in Fig. 4. *A*, examples of amperometric traces obtained from cells expressing wild type (*WT*) RLC-GFP and the unphosphorylatable double mutant T18A/S19A RLC-GFP. *B*, cumulative secretory responses were obtained from individual cell responses and averaged for cells expressing constructs of wild type RLC-GFP ($n$ = 33 cells) and T18A/S19A RLC-GFP GFP ($n$ = 22 cells).

after integration of these responses from several cells that were similar in magnitude for control uninfected and cells expressing wild type RLC-GFP (Fig. 6*B*). The number of vesicle fusions using flash stimulation was clearly reduced in cells expressing the T18A/S19A RLC-GFP, as seen in Fig. 6*A*. The responses of 16 cells were integrated, their averaged secretion profile was characterized by a 50–55% reduction in the level of secretion and an initial rate of release that changed from 8.54 ± 0.12 in wild type RLC-GFP expressing cells to 3.91 ± 0.13 picocoulomb/s in cells expressing the T18A/S19A RLC-GFP construct ($p < 0.0001$, slope calculated using the initial 5 s).

*Expression of the T18A/S19A RLC-GFP Construct Slows Single Vesicle Fusion Kinetics*—The study of individual fusion kinetics is potentially useful when looking for the mechanisms underlying the different effects of RLC-GFP constructs and can be achieved by analyzing the shape of single amperometric events (30) using carbon fiber electrodes. The analysis was performed in $BaCl_2$-stimulated cells, to search for well separated spikes with amplitudes over 2.5 pA. We measured spike amplitude ($I_{max}$), event charge ($Q$), half-width ($t_{½}$), and time-to-the-peak ($T_p$) (22). Non-infected cells or cells expressing wild type RLC-GFP were characterized by a very similar pattern of distribution, showing mean amplitudes of 68 and 73 pA, respectively (Fig. 7*A* and Table I). However, the mean amplitude obtained with mutant T18A/S19A RLC-GFP (Fig. 7*A* and Table I) was clearly reduced to half that of the control value (32 ± 5 pA). Moreover, amplitudes greater than 70 pA, which were relatively abundant in control cells were absent in this case. The observed alteration in mean amplitude did not represent a subsequent change in the amount of catecholamines released

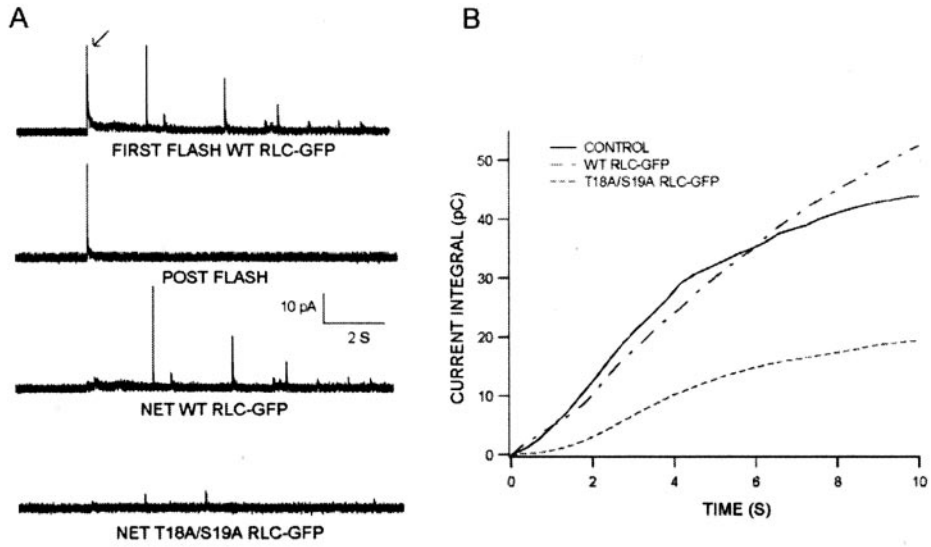


FIG. 6. **Secretory response to fast release of calcium from caged compounds in RLC-GFP expressing cells.** Secretion was monitored by amperometry as described in previous figures and exocytosis was elicited by a 5-ms flash light from a pulsatil xenon lamp in cells preincubated with 5 $\mu$M *o*-nitrophenyl-EGTA. *A*, amperometric traces representative of initial flash (*upper trace*) and post-flash responses in wild type (*WT*) RLC-GFP expressing cells. Net secretory trace obtained by subtraction of the post-flash from the initial flash. Net secretory trace representative of cells expressing T18A/S19A RLC-GFP. *B*, after building of event cumulative curves for individual cells, the average secretion was obtained from control uninfected ($n$ = 42 cells), wild type RLC-GFP ($n$ = 22 cells), and T18A/S19A RLC-GFP expressing cells ($n$ = 16).

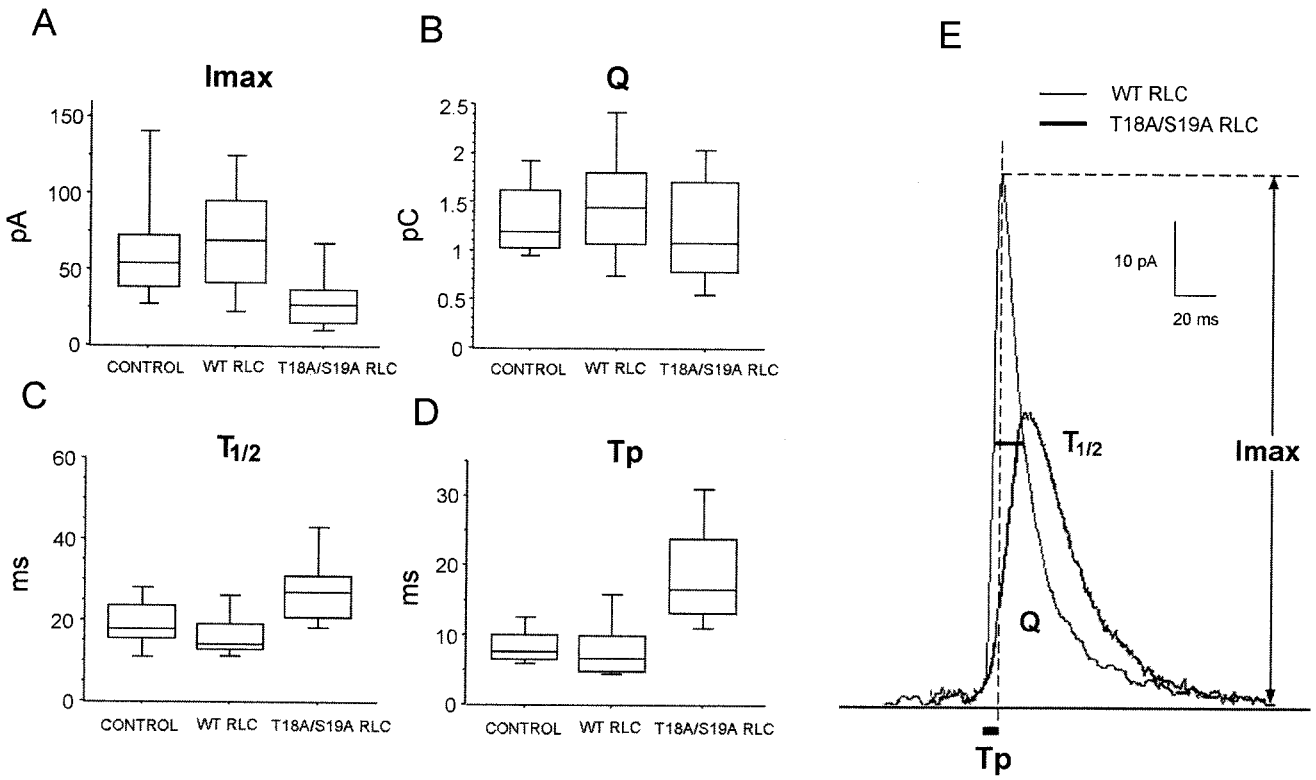


FIG. 7. **Effect of the expression of RLC-GFP constructs on single event characteristics.** Individual "spikes" were analyzed from $BaCl_2$-evoked responses of uninfected (718 events from 15 cells), wild type (*WT*) RLC-GFP expressing (858 events from 33 cells), and T18A/S19A RLC-GFP expressing cells (277 events from 22 cells). Analysis included spikes with amplitudes larger than 2.5 pA and half-widths shorter than 90 ms, to ensure that the vesicle fusions analyzed were produced in the electrode proximity. *Box plots* present 10 and 90 percentiles (*errors bars*), 25 and 75 percentiles (*box limits*), and the medians (means are given in Table I) for the amplitude values (*panel A*), event charge calculated by trapezoidal integration (*Q*, *panel B*), half-width time distributions measured by subtraction of the $t_{½}$ corresponding to the rising and falling portions of each spike ($t_{½}$, *panel C*), and time to the peak values ($T_p$, *panel D*). ***E,*** this panel shows spikes representing the average properties of events in cells expressing wild type RLC-GFP and T18A/S19A RLC-GFP constructs, in addition to showing the parameters analyzed.

per event, because the charge remained relatively unaltered in control, wild type RLC-GFP, and the double mutant T18A/S19A RLC-GFP, ranging from average values of 1.3 to 1.5 picocoulomb (Fig. 7*B* and Table I). In contrast, significant differences in the kinetics of exocytosis were observed in T18A/S19A RLC-GFP expressing cells when compared with control or the wild type RLC construct (Fig. 7*C* and Table I). Thus, the mean values for control $t_{½}$ ranged from 17 to 19 ms, whereas T18A/S19A RLC-GFP constructs had a mean value of 28.4 ± 2.0 ms (Fig. 7*C*). Similarly, the time-to-the-peak distributions

TABLE I

*Averaged parameters obtained from the analysis of individual amperometric spikes from controls and cells expressing RLC-GFP constructs*

The values were expressed as the mean ± S.E. from experiments performed in a number ($n$) of cells.

| | $I_{max}$ | Q | $T_{½}$ | $T_p$ |
|---|---|---|---|---|
| | *pA* | *pC* | *ms* | |
| Control ($n$ = 15 cells, 718 spikes) | 68 ± 14 | 1.4 ± 0.1 | 19.7 ± 1.7 | 8.6 ± 0.7 |
| WT RLC-GFP ($n$ = 33 cells, 858 spikes) | 73 ± 7 | 1.5 ± 0.1 | 16.7 ± 1.1 | 9.4 ± 1.4 |
| T18A/S19A RLC-GFP ($n$ = 22 cells, 277 spikes) | 32 ± 5[a] | 1.3 ± 0.2 | 28.4 ± 2.0[a] | 19.5 ± 1.9[a] |
| Control, 10 μM ML-9 ($n$ = 21 cells, 243 spikes) | 31 ± 2[a] | 1.2 ± 0.2 | 27.9 ± 1.7[a] | 12.9 ± 0.9[b] |

[a] $p < 0.0001$ using the non-parametric Mann-Whitney test compared with the wild type RLC-GFP values for a given number of cells.
[b] $p < 0.001$ using the non-parametric Mann-Whitney test compared with the wild type RLC-GFP values for a given number of cells.

were characterized by larger values in the RLC non-phosphorylatable mutant (19.5 ms mean value) compared with 8.5 and 9.4 ms for the control and wild type RLC-GFP construct, respectively. It is clear from the modifications in single vesicle fusion parameters, that the secretory events found in cells expressing the T18A/S19A RLC-GFP construct were considerably slower than control or wild type RLC-GFP expressing cells, while maintaining the charge released per event (Fig. 7*E*). These data demonstrate that myosin II activity influences the very final events linked to the exocytotic fusion of membranes and the release of catecholamines in this neuroendocrine cell model. In agreement with this conclusion, we have observed that control cells incubated with 10 μM ML-9 for 15 min secreted catecholamines with significantly slower individual granule fusion kinetics (Table I), thus mimicking the effect caused by the expression of the non-phosphorylatable form of RLC-GFP.

## DISCUSSION

In this study, we have found that the expression of an unphosphorylatable form of myosin II RLC-GFP severely modified the vesicle mobility properties and secretory capability of bovine chromaffin cells in culture. Interestingly, the alteration of the initial phase of secretion in cells stimulated by different secretagogues, and in the fast components of secretion after calcium release from caged compounds, demonstrates that myosin II modulates the fusion of ready releasable vesicles. This unexpected result is further supported by the finding that expression of this double mutant also modifies the kinetics of exocytosis of individual vesicles analyzed by amperometry.

An important finding of our study is that the expression of wild-type RLC-GFP allows both normal vesicle transport activity and characteristics of secretion in bovine chromaffin cells in culture, thereby validating the use of this construct as a template to study the effects of specific mutations on the secretory cycle. In effect, the mobility of vesicles visualized by dynamic confocal microscopy of quinacrine-loaded granules matched closely that found in control-uninfected cells. This high mobility is characteristic of cytosolic granules in intact chromaffin cells (2) and produced an average displacement in the *xy* plane of 3–4 μm/20 s with a diffusion coefficient estimated to be 7–10 × $10^{-3}$ $\mu m^2/s$, very similar to that estimated for the "mobile" population of vesicles using TIRFM (31, 32). In addition, expression of the wild type RLC-GFP construct sustained the exocytotic properties of bovine chromaffin cells, because its secretory capability and kinetic profiles during single cell stimulation were similar to the control cells not expressing this construct. These results also coincided with the average secretory capability and single fusion kinetics described for amplicon-infected chromaffin cells in previous works (27). These results support the idea that the expressed RLC interacted with endogenous myosin II heavy chain and therefore co-localized with cortical F-actin as reported here. Myosin II localization in the cell cortex has been described by different groups (12, 13). In addition, the capability of the RLC-GFP chimeric protein in binding stoichiometrically to smooth muscle RLC-deficient myosin II has been described, and supports the actin-activated ATPase activity of myosin modulated by MLCK phosphorylation (15).

In contrast, expression of the double mutant chimera T18A/S19A RLC-GFP, which yields an unphosphorylatable form of myosin II by MLCK and precluding activation of its motor activity (8), affected the physiology of chromaffin cells in various ways. First, granule transport in the cytosol was clearly diminished reaching a restriction in mobility that was similar to that obtained by incubation of cells with the F-actin stabilizer phalloidin and even higher restriction than that reached in the presence of the nonspecific myosin inhibitor BDM (2, 12, 31). This clearly suggests that expression of this construct produces a static network of F-actin incapable of sustaining the normal transport of vesicles and therefore the mechanism of myosin II regulation by RLC phosphorylation by MLCK appears to be essential to F-actin dynamics in this neuroendocrine model. Second, cells expressing this construct also manifested altered secretory properties when individual cells were challenged by KCl depolarization in the presence of $BaCl_2$, two secretagogues that appeared to recruit populations of granules at different stages of maturation (33). Unexpectedly, inhibition of secretion affected the initial rate of release as shown in Figs. 4 and 5. The alteration of a protein implicated in vesicle transport was expected to preferentially influence slow phases of secretion leaving the initial secretory burst almost unaffected. This secretory pattern has been observed when low concentrations of BoNT A selectively affected the release of undocked vesicles (18). This observation is further supported when the initial rate of vesicle fusion after uncaging $Ca^{2+}$ was also affected in cells expressing the unphosphorylatable form of RLC-GFP. In this case, the fast and homogeneous rise in calcium ensured the release of the ready releasable granules. These results, which demonstrate an alteration in the initial rate of release, agree with previous data showing an alteration of ATP-independent secretion with wortmannin in permeabilized chromaffin cells (11, 34) or BDM affecting the rate of release of permeabilized and intact cells (2, 12). Another demonstration of the alteration of myosin II activity by expression of an unphosphorylatable form affecting the release of matured docked vesicles was provided by the analysis of individual fusion kinetics from amperometric recordings. It has been shown that the statistical analysis of the parameters defining the shape of amperometric spikes reflects the kinetics of single vesicle fusion (30). The average characteristics of lower amplitude, increased $t_{½}$, and equal charge released per amperometric event found in T18A/S19A RLC-GFP expressing cells indi-

cate a slower kinetics of single granule fusion in the presence of the unphosphorylatable form of myosin II, an effect that has been found also when control cells were treated with ML-9. This might imply that myosin II activity influenced either the kinetics of exocytotic pore expansion or the degree of neurotransmitter dissociation from the vesicular matrix. It is unlikely that myosin II could influence processes taking place in the interior of the vesicular matrix, therefore we favor the first possibility. How could myosin II influence the very final phases of membrane fusion? It has been shown that this cytoskeletal protein is associated with the F-actin network (12, 34), and that even the most external docked granules remain associated with filaments of this mesh (2), therefore the requirements for an appropriated spatial coincidence between matured vesicles and myosin II seems to be possible. In that way, myosin II may exert a tensional pressure in the F-actin network thereby affecting membrane tension, fusion pore expansion, and finally, extrusion of vesicular contents. Alternatively, myosin II might be able to influence the activity of the molecular machinery of exocytosis. In this sense, an association has been demonstrated between the tail of the heavy chain of unconventional myosin V and synaptobrevin II forming part of the exocytotic fusion complex in synaptic vesicles (35). Therefore as a second possibility, it is tempting to suggest that myosins, through interactions with synaptobrevin or other proteins of the fusion machinery, could be modulating the series of transitions occurring in the exocytotic fusion complex and could be modulating the priming or maturation membrane-bound steps of secretory vesicles (36).

In conclusion, the present work demonstrates that cytoskeletal elements such as conventional myosin II affect different stages of the exocytotic process and not merely the transport of vesicles. Orienting research toward these newly proposed interactions may help to clarify and unravel some of the complex aspects of the exocytotic cycle.

*Acknowledgment*—We thank Stuart Inham for style corrections.

REFERENCES

1. Viveros, O. H. (1974) in *Handbook of Endocrinology* (Blasko, H., Sayers, G., and Smith, A. D., eds) pp. 389–426, American Physiology Society, Baltimore, MD
2. Ñeco, P., Giner, D., Francés, M. M., Viniegra, S., and Gutiérrez, L. M. (2003) *Eur. J. Neurosci.* **18,** 733–742
3. Perrin, D., and Aunis, D. (1985) *Nature* **315,** 589–591
4. Cheek, T. R., and Burgoyne R. D. (1986) *FEBS Lett.* **207,** 110–114
5. Coté, A., Doucet, J-P., and Trifaró, J-M. (1986) *Neuroscience* **19,** 629–645
6. Gutiérrez, L. M., Ballesta, J. J., Hidalgo, M. J., Gandía, L., García, A. G., and Reig, J. A. (1988) *J. Neurochem.* **51,** 1023–1030
7. Gutiérrez, L. M., Hidalgo, M. J., Palmero, M., Ballesta, J. J., Reig, J. A., García, A. G., and Viniegra, S. (1989) *Biochem. J.* **264,** 589–596
8. Kamm, K. E., and Stull, J. T. (1989) *Annu. Rev. Physiol.* **51,** 299–313
9. Lee, S. A., Holz, R. W., and Hathaway, D. R. (1987) *Biosci. Rep.* **7,** 323–332
10. Nakanishi, A., Yoshizumi, M., Hamano, S., Morita, K., and Oka, M. (1989) *Biochem. Pharmacol.* **38,** 2615–2619
11. Ohara-Imaizumi, M., Sakurai, T., Nakamura, S., Nakanishi, S., Matsuda, Y., Muramatsu, S., Nomura, Y., and Kumakura, K. (1992) *Biochem. Biophys. Res. Commun.* **185,** 1016–1021
12. Ñeco, P., Gil, A., Francés, M. M., Viniegra, S., and Gutiérrez, L. M. (2002) *Biochem. J.* **368,** 405–413
13. Rosé, S. D., Lejen, T., Casaletti, L., Larson, R. E., Pene, T. D., and Trifaró, J. M. (2003) *J. Neurochem.* **85,** 287–298
14. Rudolf, R., Kogel, T., Kuznetsov, S. S., Salm, T., Schlicker, O., Hellwig, A., Hammer, J. A., 3rd, and Gerdes, H. H. (2003) *J. Cell Sci.* **116,** 1339–1348
15. Komatsu, S., Yano, T., Shibata, M., Tuft, R. A., and Ikebe, M. (2000) *J. Biol. Chem.* **275,** 34512–34520
16. Lim, F., Hartley, D., Starr, P., Lang, P., Song, S., Yu, L., Wang, Y., and Geller, A. Y. (1996) *BioTechniques* **20,** 460–469
17. Almazán, G., Aunis, D., García, A. G., Montiel, C., Nicolás, G. P., and Sanchez-García, P. (1984) *Br. J. Pharmacol.* **81,** 599–610
18. Gíl, A., Viniegra, S., and Gutiérrez, L. M. (1998) *Eur. J. Neurosci.* **10,** 3369–3378
19. Criado, M., Gil, A., Viniegra, S., and Gutiérrez, L. M. (1999) *Proc. Natl. Acad. Sci. U. S. A.* **96,** 7256–7261
20. Gíl, A., Rueda, J., Viniegra, S., and Gutiérrez, L. M. (2000) *Neuroscience* **98,** 605–614
21. Kawagoe, K. T., Zimmerman, J. B., and Wightman, R. M. (1993) *J. Neurosci. Methods* **48,** 225–240
22. Segura, F., Brioso, M. A., Gómez, J. F., Machado, J. D., and Borges, R. (2000) *J. Neurosci. Methods* **103,** 151–156
23. Grynkiewicz, G., Poenie, M., and Tsien, R. Y. (1985) *J. Biol. Chem.* **260,** 3440–3450
24. Haller, T., Auktor, M., Frick, M., Mair, N., and Dietl, P. (1999) *Am. J. Physiol.* **277,** L893–L900
25. Qian, H., Sheetz, M. P., and Elson, E. L. (1991) *Biophys. J.* **60,** 910–921
26. Lazarides, E. (1976) *J. Cell Biol.* **68,** 202–219
27. Gíl, A., Gutiérrez, L. M., Carrasco-Serrano, C., Alonso, T., Viniegra, S., and Criado, M. (2002) *J. Biol. Chem.* **277,** 9904–9910
28. Ludowyke, R. I., Peleg, I., Beaven, M. A., and Adelstein, R. S. (1989) *J. Biol. Chem.* **264,** 12492–12501
29. Ellis-Davies, G. C., and Kaplan, J. H. (1994) *Proc. Natl. Acad. Sci. U. S. A.*, **91,** 187–191
30. Schroeder, T. J., Borges, R., Finnegan, J. M., Amatore, C., Pihel, K., and Wightman, R. M. (1996) *Biophys. J.* **70,** 1061–1068
31. Lang, T., Wacker, I., Wunderlic, I., Rohrbach, A., Giese, G., Soldati, T., and Almers, W. (2000) *Biophys. J.* **78,** 2863–2877
32. Oheim, M., and Stühmer, W. (2000) *Eur. Biophys. J.* **29,** 67–89
33. Duncan, R. R., Greaves, J., Wiegand, U. K., Matskevich, I., Bodammer, G., Apps, D. K., Shipston, M. J., and Chow, R. H. (2003) *Nature* **422,** 176–180
34. Kumakura, K., Sasaki, K., Sakurai, T., Ohara-Imaizumi, M., Misonou, M., Nakamura, S., Matsuda, Y., and Nonomura, Y. (1994) *J. Neurosci.* **14,** 7695–7703
35. Prekeris, R., and Terrian, D. M. (1997) *J. Cell Biol.* **137,** 1589–1601
36. Südhof, T. C. (1995) *Nature* **375,** 645–653